# Adaptive Power Sharing and Switching Frequency Control for Power Loss Optimization in WBG/Si Hybrid Half-Bridge Converters

Chao Zhang, *Member, IEEE*, Xufeng Yuan, *Member, IEEE*, Jun Wang, *Senior Member, IEEE*, Weibin Chen, Bo Hu, *Graduate Student Member, IEEE*, and Zheng John Shen, *Fellow, IEEE*

***Abstract*—The optimization of switching frequencies and the power-sharing ratio between the silicon (Si) phase and wide-bandgap (WBG) phase are critically important for the efficiency improvement and safe operation of the WBG/Si hybrid half-bridge (HHB)-based power converters. In this article, a novel adaptive power sharing and switching frequency control for power loss optimization in WBG/Si HHB is proposed. It is based on intelligence particle swarm optimization (PSO), especially suitable for applications with time-varying operation current. The PSO approach only evaluates the fitness values to seek the best optimal parameters without requiring an accurate power loss model and additional hardware components. Therefore, the proposed method can be easily implemented and adapted to various working conditions. A 3-kW prototype of the Si/SiC HHB-based single-phase inverter is built to validate the proposed approach. In comparison with the fixed frequency and power-sharing ratio, the proposed method achieves an 18% maximum total power loss reduction while maintaining the same power quality performance.**

***Index Terms*—Adaptive control, hybrid Si/WBG, power loss optimization, power sharing optimization, particle swarm optimization.**

## I. Introduction

THE WBG/Si hybrid half-bridge (HHB) consists of a small-capacity WBG phase and a high-capacity Si phase, which is coordinated by a hybrid-frequency interleaving operation to provide an improved tradeoff between cost and performance [1], [2], [3], [4]. Fig. 1 shows the diagram and topology of the WBG/Si HHB approach, in which the WBG phase process a fractional of the total power at a high frequency to achieve the high quality of the whole converter, whereas the low-cost Si phase processes most of the total power at an extremely low frequency to reduce the switching losses. Therefore, it is perceived as the key enabler of high frequency, high efficiency, and low cost in the application of high-power converters, especially in high-current applications [5], [6], [7], [8], [9].

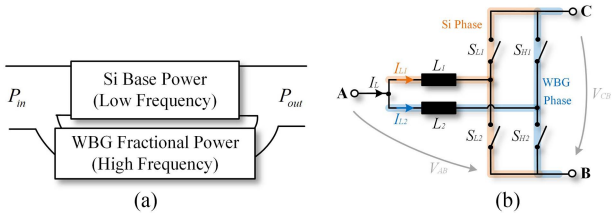


Fig. 1. Diagram and topology of the WBG/Si HHB approach. (a) Diagram of the WBG/Si HHB. (b) Topology of the WBG/Si HHB.

Due to the unique hybrid-frequency interleaving operation for WBG/Si HHB-based converters, the switching frequencies and power-sharing between those two phases can seriously affect the efficiency performance. On the one hand, the lower the Si phase switching frequencies, the lower the Si phase switching losses, but the larger current ripple will increase conduction losses. On the other hand, different power-sharing ratios will seriously affect the safe operation of those two phases, and the overall power loss since the electrical characteristics (switching and conduction characteristics) of the two phases are completely different. Therefore, the proper selection of the switching frequencies and power-sharing between those two phases are critically important for the efficiency improvement of the WBG/Si HHB-based power converters.

Most previous research only chose a preliminarily reasonable fixed switching frequency and power-sharing ratio to experimentally demonstrate the electrical performance benefits of the HHB solution or only discussed fixed optimal parameters from an offline power loss model. Kundu et al. [10], [11] reported a hybrid Si/SiC voltage source inverter design, in which the current sharing ratio is delivered as 1: 2 from a simple loss model, and the frequency is fixed to 2/10 kHz. In [12] and

Manuscript received 20 July 2022; revised 28 October 2022; accepted 13 December 2022. Date of publication 20 December 2022; date of current version 14 February 2023. This work was supported in part by the Guidateganghezi Project under Grant TGHZ 2022[45], in part by the National Key Research and Development Program of China under Grant 2022YFE0205300, in part by the Guizhou Provincial Science and Technology Projects under Grant ZK [2022] General 154 and under Grant [2022] General 012, and in part by the National Natural Science Foundation of China under Grant 52067004, Grant 52167007, Grant 51977068. Recommended for publication by Associate Editor C. DiMarino. *(Corresponding author: Xufeng Yuan.)*

Chao Zhang and Xufeng Yuan are with the Electrical Engineering College, Guizhou University, Guiyang 550025, China (e-mail: zhangc@gzu.edu.cn; xfyuan@gzu.edu.cn).

Jun Wang, Weibin Chen, and Bo Hu are with the College of Electrical and Information Engineering, Hunan University, Changsha 410012, China (e-mail: junwang@hnu.edu.cn; 2545622700@qq.com; dfs_hb@163.com).

Zheng John Shen is with the School of Mechatronic Systems Engineering, Simon Fraser University, Surrey, BC V3T 0A3, Canada (e-mail: zjohnshen@gmail.com).

Color versions of one or more figures in this article are available at https://doi.org/10.1109/TPEL.2022.3230747.

Digital Object Identifier 10.1109/TPEL.2022.3230747

[13], a hybrid Si/SiC totem-pole bridgeless PFC converter is designed with a fixed switching frequency of 20/160 kHz and a dynamic power-sharing ratio. But this dynamic power-sharing ratio is only designed to ensure the safe operation of the SiC phase, instead of optimization for the total loss minimization. Recently, Zhang et al. [14] developed an accurate power loss of the WBG/Si HHB through the double-pulse test and system parameters, and then a lookup table (LUT) is used to select the optimal Si phase switching frequency and power-sharing ratio according to different operating conditions. However, the establishment of the power loss model is based on a single operation state, and the different operation states of the power electronics system are not considered. It means that the proposed methods in these papers are only suitable for the dc–dc converter, where both the current and the device junction temperature are almost constant. While in ac applications, such as ac–dc or dc–ac, the junction temperature, and the operation current of the HHB, are time-varying [15], [16], resulting in a large variation in the optimal combinations of switching frequency and power sharing. Therefore, it is very difficult and complex to obtain the optimal parameters by offline power loss modeling and computation. It is necessary to explore a new simple, effective approach to regulating the switching frequency and power-sharing ratio adaptively for power loss minimization.

In this article, a novel adaptive power-sharing and switching frequency control for power loss optimization for WBG/Si HHB is proposed, which is based on intelligence particle swarm optimization (PSO) and does not require the complex accurate power loss model and the additional hardware components. The proposed adaptive optimization process is only guided by a simple fitness function. Therefore, it can simply and effectively achieve the efficiency improvement of the WBG/Si HHB-based converters (including the dc/dc, dc/ac, and ac/dc) and adapt to various working conditions. The Si/SiC HHB-based dc–ac inverter is selected as a verification case, and its time-varying sinusoidal current not only illustrates the general implementation process and advantages of the proposed adaptive PSO control, but also further demonstrates the design process and benefits of the multi-particle dimension optimization.

The rest of this article is organized as follows. In Section II, the topology and basic operation of the HHB approach are introduced. Then, the technology challenges for adopting the HHB approach are analyzed. In Section III, the adaptive optimization strategy is presented, which includes the optimization variables selection, the principle and working flow of the PSO, the calculation burden analysis, and the discussion of load-variation conditions. Experiments are presented in a single-phase inverter case study in Section IV. Finally, Section V concludes this article.

## II. Topology and Operation Analysis

In this section, the operation principle of the WBG/Si HHB approach is presented. Then, the major challenges of seeking the optimal switching frequency and power-sharing ratio are analyzed. The details are as follows.

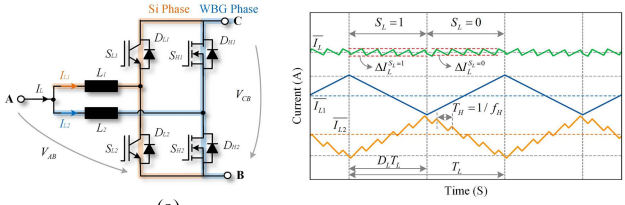


(a) (b)

Fig. 2. Topology and current waveforms for WBG/Si HHB. (a) Topology. (b) Current waveforms.

### A. Operation Principle

Fig. 2(a) shows the topology of the WBG/Si HHB, which comprises a large-capacity Si phase and a small-capacity WBG phase. The Si phase operates at a low frequency to lightly process most of the total current, obtaining a high-efficiency base power path. But the low-frequency operation will result in a large current ripple, shown by the yellow line in Fig. 2(b). The WBG phase operates at a high frequency to cancel the Si phase current ripple in terms of processing a fractional of the total current. The WBG phase current waveforms are shown by the blue line in Fig. 2(b), which has a small average value and a low-frequency ripple with an opposite phase to the Si phase. After canceling the Si phase current ripple, the total current only exhibits the small high-frequency ripple as the full high-frequency WBG phase. Therefore, the WBG/Si HHB can achieve near the same high-quality benefits as the all-WBG design by only using a small capacity WBG phase, achieving an improved tradeoff between cost and performance.

Based on the current waveforms in Fig. 2(b), the relations of those currents can be expressed as

$$\begin{cases} \overline{I_{L1}} = K\overline{I_L} \\ \overline{I_{L2}} = (1-K)\,\overline{I_L} \\ \Delta I_{L1} = \frac{V_{AB} D_L}{L_1 f_L} \\ \Delta I_{L2} = \Delta I_{L1} \end{cases} \tag{1}$$

where $\overline{I_L}$, $\overline{I_{L1}}$, and $\overline{I_{L2}}$ are the average current for total, Si phase, and WBG phase, respectively. $K$ is the power-sharing ratio, which determines the power-sharing of those two phases. $\Delta I_{L1}$ is the Si phase current ripple, which is related to the Si phase duty cycle $D_L$ and switching frequency $f_L$. The WBG phase current ripple $\Delta I_{L2}$ equals the $\Delta I_{L1}$ to achieve the full compensation for the Si phase current ripple.

### B. Power Loss Analysis for HHB

The Si phase power loss consists of the loss in switching devices and inductors, and the brief formula can be expressed as

$$P_{\mathrm{Si}} = P_{\mathrm{Si},cond} + P_{\mathrm{Si},sw} + P_{L1,cu} + P_{L1,core} \tag{2}$$

where $P_{\mathrm{Si,cond}}$ and the $P_{\mathrm{Si,sw}}$ are the conduction and switching losses for Si devices, respectively. $P_{L1,\mathrm{cu}}$ and $P_{L1,\mathrm{core}}$ are the copper and core losses for inductor $L_1$. All those parts are related to Si phase switching frequency and power-sharing ratio, which

can briefly be expressed according to the reference [14]

$$\begin{cases} P_{\mathrm{Si},cond} = \left(V_{ce} + I_{L1,\mathrm{rms}}\left(f_L,K\right)R_{ce}\right) I_{L1,\mathrm{rms}}\left(f_L,K\right) D_L \\ \qquad\qquad + \left(V_d + I_{L1,\mathrm{rms}}\left(f_L,K\right)R_d\right) \\ \qquad\qquad \times I_{L1,\mathrm{rms}}\left(f_L,K\right)\left(1-D_L\right) \\ P_{Si,sw} = \left(E_{\mathrm{Si},on}\left(f_L,K\right) + E_{\mathrm{Si},off}\left(f_L,K\right)\right. \\ \qquad\qquad \left. + E_{\mathrm{Si},rec}\left(f_L,K\right)\right) f_L \\ P_{L1,\mathrm{cu}} = I^2_{L1,\mathrm{rms}}\left(f_L,K\right) R_{L1,\mathrm{cu}} \\ P_{L1,\mathrm{core}} = V_c K_c f_L^{\alpha}\left(\frac{\Delta B(f_L,K)}{2}\right)^{\beta} \end{cases} \tag{3}$$

where $V_{ce}$ and $R_{ce}$ are the knee voltage and equivalent ON-state resistance for the IGBTs, and $V_d$ and $R_d$ are the knee voltage and equivalent ON-state resistance for the Si diode. $I_{L1,\mathrm{rms}}$ is the Si phase rms current, which is related to the $f_L$ and $K$. $E_{\mathrm{Si,on}}$, $E_{\mathrm{Si,off}}$ and $E_{\mathrm{Si,rec}}$ stands for the switch-ON, switch-OFF, and recovery energy, which are the function of the $f_{SL}$ and $K$. $R_{L1,\mathrm{cu}}$ is the equivalent resistance of the inductor $L_1$. $K_c$, $\alpha$, and $\beta$ are the fit parameters, which can be found in the core datasheets [17]. $V_c$ stands for the volume of the core. Meanwhile, the characteristics of the inductors and devices are strongly dependent on junction temperature. Thus, the power loss for each component in the Si phase is not only related to $f_L$ and $K$, but also related to the junction temperature, i.e.,

$$P_{\mathrm{Si}} = f\left(f_L, K, T_j\right). \tag{4}$$

Similarly, the power loss of the WBG phase also includes the switching devices and inductors, which is related to its operation frequency $f_H$ and current $I_{L2}$. At the same time, the WBG phase current must compensate for the Si phase current ripple. Therefore, the power loss of the WBG phase will not only be influenced by $f_H$ and power-sharing ratio but also be severely affected by the Si phase switching frequency $f_L$ and $T_j$, i.e.,

$$P_{\mathrm{WBG}} = f\left(f_L, K, f_H, T_j\right). \tag{5}$$

In conclusion, the total power loss of the WBG/Si HHB is mainly affected by the following three parameters.

1) *Si phase switching frequency $f_L$:* The Si phase switching frequency does not only affect the power loss of the Si phase, but also affects the WBG phase. Lower switching frequency means lower switching losses for Si devices. But the larger current ripple caused by the low-frequency operation will increase the losses in the inductor and WBG phase.
2) *Power-sharing ratio K:* The power-sharing ratio determines the average current processed by the Si phase, enabling a free power-sharing ratio. Since the characteristics of the two phases are quite different, the $K$ can seriously affect the total loss of HHB. The selection of the power-sharing ratio $K$ requires comprehensive consideration of the loss distribution of those two phases to minimize the total loss.
3) *WBG phase switching frequency $f_H$:* Higher WBG phase switching frequency, lower current ripple, and smaller ripple losses result in larger switching losses. Since the WBG phase switching frequency directly determines the total current performance, it must be selected based on the total current ripple requirements.

### C. Technology Challenges for Conventional Optimization

It is important to select an optimal power-sharing ratio and switching frequency to minimize power loss. Conventional methods mainly focus on a power loss model-based optimization strategy, which obtained the fixed optimal system parameter design by offline power loss model analysis. However, there are several technical challenges in those power loss model-based optimization strategies.

1) The establishment of an accurate device loss model is difficult and complex. In WBG/Si HHB, the Si phase frequency is deliberately reduced to avoid excessive switching losses, but this leads to a larger current ripple. Therefore, the effect of the current ripple on the power loss cannot be ignored as in the previous literature. Considering the skin effect of the inductor at different frequencies and the temperature-dependent switching characteristics of different devices, the accurate loss modeling process is very time-consuming and complex.
2) An accurate loss model needs additional components cost. The switching characteristics for all devices are temperature dependent and may require additional temperature sensors to capture the environmental temperature of the system to achieve accurate loss estimates, which will increase the components' cost and decrease the system power density.
3) The optimal design parameters are varied under different operation conditions. The optimal design parameters are coupled with the junction temperature, inductor losses, and current ripples. Furthermore, those three parameters are coupled with each other. For example, the optimal power-sharing ratio is a varied different combination of the different switching frequencies. Therefore, the conventional offline losses model-based optimization method cannot cover all the operation conditions, and the applicability is limited.

In summary, it is difficult to obtain the optimal time-varying power-sharing ratio and switching frequency by the conventional power loss model method, the optimal parameters design cannot be easily obtained offline.

## III. Adaptive Power Loss Optimization Strategy

To address those challenges, an adaptive power-sharing ratio and switching frequency control are proposed, which adopts the PSO algorithm for online multivariable optimization to minimize the whole system power losses. The operation principle, optimization variables selection, and implementation flow of the PSO algorithm are presented in the following.

### A. Operation Principle of PSO

The PSO is an evolutionary computation technique proposed by Dr. Eberhart and Dr. Kennedy in 1995 [18], which originated from bird predation behavior. The basic idea of the PSO

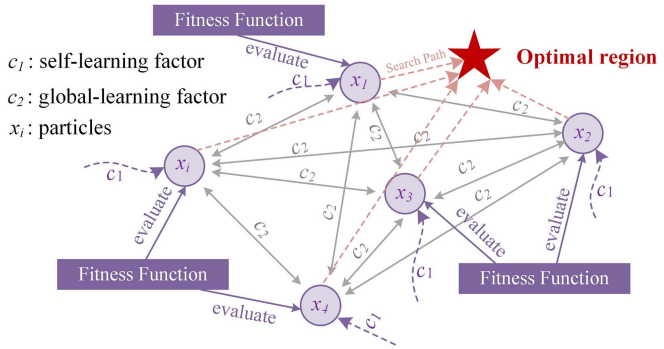


Fig. 3. Operation principle of the PSO algorithm.

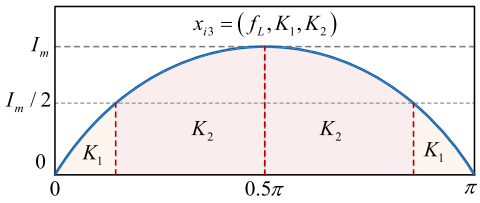


Fig. 4. Particle coding of the PSO algorithm: 3-D coding is taken as an example. The power-sharing ratio can be varied twice in a quarter of a fundamental cycle, which means that there are three dimensions ($f_L$, $K_1$, and $K_2$) for each particle.

algorithm is to find the optimal solution through collaboration and information sharing between individuals (particles) in the group, as shown in Fig. 3. Benefits from its simple and easy implementation, fast convergence speed, and no requirement of an exact model, the PSO algorithm has been widely used in the application fields of function optimization, neural network training, power system control, and other genetic algorithms [19], [20], [21].

The previous publication indicates that the total power quality is only related to the WBG phase switching frequency in WBG/Si HHB [1], thus the WBG phase switching frequency is fixed to obtain a stable power quality for the whole HHB. Further, there are at least two dimensions ($f_L$, $K$) that need to be considered in PSO. Since the current in dc–dc applications is constant under one fixed operating condition, the power-sharing ratio can be regarded as a constant value, i.e., PSO has two dimensions. While the current is a time-varying sinusoidal current in ac–dc applications, the power-sharing ratio can be varied several times during a line cycle. Fig. 4 shows the example in a sinusoidal current with two power-sharing ratios in a quarter of a fundamental cycle, thus the PSO should be configured as three dimensions, which can be expressed as

$$x_i = (x_{i1}, \ldots, x_{id}) = (f_L, K_1, K_2) \tag{6}$$

where $x_{id}$ ($i$ is the number of particles and $d$ is the dimension of the particle) stands for the individual particle, and the corresponding particle velocity is the $V_i$. Assuming that $x_i$ ($m$) and $v_i$ ($m$) represent the position and velocity of particle $x_i$ at the $m$th iteration in the swarm, the updated procedure of PSO relies on the historical particle position, and the new velocity and new position can be updated as

$$\begin{cases} v_i(m+1) = wv_i(m) + c_1 r_1 (p_{\text{best},i} - x_i(m)) \\ \qquad\qquad + c_2 r_2 (g_{\text{best},i} - x_i(m)) \\ x_i(m+1) = x_i(m) + v_i(m+1) \end{cases} \tag{7}$$

where $r_1$ and $r_2$ are random numbers between 0 and 1, $c_1$ and $c_2$ are the learning factor for the individual and global particles, respectively, $m$ is the number of current iterations, $P_{\text{best},i}$ is the local best at the $m$th iteration of the personal particle, and $g_{\text{best},i}$ represents the global best of all particles. $\omega$ is the iteration weight factor, which affects the next particle's velocity by comparing it with the previous particle's velocity and represents the searchability of the particle. In general, the larger the $\omega$ is, the stronger the initial global searchability, but the lower the search velocity, and vice versa. Thus, the inertia weight is general the time-varying parameter to keep a balance between searchability and velocity. The more commonly used strategy is the linear decreasing weights strategy [21], i.e.,

$$w(m) = w_{\max} - (w_{\max} - w_{\min}) \frac{m}{N} \tag{8}$$

where $\omega_{\max}$ and $\omega_{\min}$ stand for the maximum and minimum weight factor, $m$ is the current number of the inertia, and $N$ is the maximum number of inertia.

For each iteration, the particles' positions are updated, and a fitness function $P_{\text{loss}}(x)$ is introduced as the judgment of the swarm. The optimization problem here is to minimize the power losses of the whole inverter. Therefore, the average total loss is set as the fitness function, and the specific value of the power loss will not be incorporated into the PSO calculation process, but only used to compare the power loss performance under different particles. Therefore, the proposed algorithm only needs to reflect the variation trend of power loss under different particle parameters. The average power loss could be mathematically expressed as

$$P_{\text{loss}}(x_i) = P_{\text{in}} - P_{\text{out}} = \frac{1}{T_s}\int_0^{T_s} V_{\text{in}} I_{\text{in}} dt - \frac{1}{T_s}\int_0^{T_s} V_o I_o dt \tag{9}$$

where $P_{in}$ and $P_o$ stand for the input power and output power, respectively. $V_{\text{in}}$ and $I_{\text{in}}$ stand for the input voltage and current, $V_o$ and $I_o$ stand for the output voltage and current. $T_s$ represents the operating period of the converter, which can be using the half or whole gird line cycle period in ac applications. In the actual digital signal processor (DSP) or field programmable gate array (FPGA) implementation stage, the integral-averaged operation can be realized by a discrete moving-average function to meet the loss comparison requirements of the proposed PSO algorithm. Thus, the fitness function can be obtained by the measured data without an additional complex power loss model. The particles (different combinations of $f_L$, and $K_i$) in the swarm hyperspace will produce a fitness result, and here is the system power loss. The minimized individual and global fitness positions are recorded to the next iterations and end when the fitness function is minimized or reaches the maximum number of iterations.

### B. Optimization Range

The key issue for implementing PSO optimization is to choose the proper range of dimensions. The selection principle of the

optimization variables is that the online dynamic updating of the variables will not affect the quality and increase additional issues of the total output current.

The optimization range of the Si phase switching frequency is selected. On the one hand, the Si phase switching frequency must be higher than 10 kHz to avoid generating acoustic noise and make the converter quiet in operation. On the other hand, the Si phase switching frequency must be lower than 30 kHz to avoid excess switching losses. However, the system stability may be affected by a varied switching frequency operation. Therefore, after a preliminary frequency range has been selected, a stability analysis must be performed to verify that the range is appropriate, which can be completed by establishing a discrete small-signal model of the converter and judging by the amplitude of the characteristic root [22], [23], [24].

The WBG phase switching frequency directly determines the total current performance. Thus, the WBG phase switching frequency must be selected based on the total current ripple requirements. Our previous publication [1] has indicated that the total current exhibits two ripple behaviors according to different Si phase switching functions and can be delivered the total current peak-to-peak ripple as follows:

$$\begin{cases} \Delta I_L^{S_L=0} = \frac{(V_{CB}-V_{AB})(L_1+L_2)(L_1V_{AB}+L_2V_{AB}-L_2V_{CB})}{L_1^2L_2V_{CB}f_H} \\ \Delta I_L^{S_L=1} = \frac{-V_{AB}(L_1+L_2)(L_1V_{AB}+L_2V_{AB}-L_1V_{CB})}{L_1^2L_2V_{CB}f_H} \end{cases} \tag{10}$$

where $S_L$ is the Si phase switching function, $S_L = 1$ stands for $S_{L1}$ is ON and $S_{L2}$ is OFF, and vice versa. $L_1$ and $L_2$ are the Si phase and WBG phase inductances. $f_H$ is the WBG phase switching frequency. The maximum peak-to-peak value must be lower than the ripple requirements, i.e.,

$$\max\left(\Delta I_{L1}^{S_L=1}, \Delta I_{L1}^{S_L=0}\right) \le r_L\overline{I_L} \tag{11}$$

where $r_L$ is the allowable ripple ratio for total current. The WBG phase switching frequency can be obtained by an inverse solution and fixed to achieve a stable power quality for the whole HHB. Therefore, the proposed PSO algorithm does not require capturing and optimizing the current ripple performance in every switching period, which is ensured by the fixed WBG phase switching frequency and benefits from the unique operation of the WBG/Si HHB.

The range selection of the power-sharing ratio must ensure that the WBG phase always operates within the safe operation area (SOA). As indicated in Fig. 2, the peak current for WBG phase current can be obtained as

$$I_{L2,\text{peak}} = (1-K)\overline{I_L} + \Delta I_{L1}/2. \tag{12}$$

To ensure safe operation, $I_{L2,\text{peak}}$ must be smaller than the safety operation current for WBG devices, i.e.,

$$I_{L2,\text{peak}} \le I_{\text{soa}} \tag{13}$$

where $I_{\text{soa}}$is the SOA current for the selected WBG device. Thus, the power-sharing ratio optimization range can be expressed as

$$K \in \left[1 - \frac{I_{\text{soa}} - \Delta I_{L1}/2}{\overline{I_L}}, 1\right]. \tag{14}$$

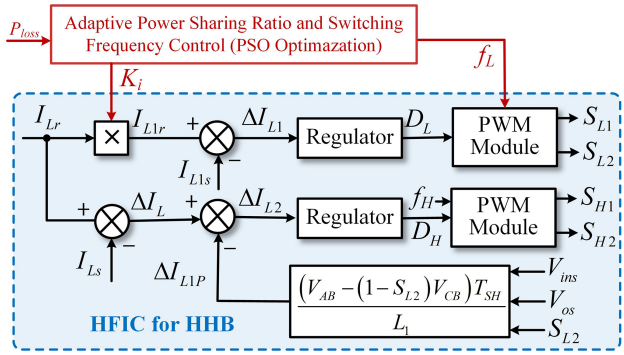


Fig. 5. Proposed adaptive power sharing ratio and switching frequency control.

By the proper selection of the optimization ranges, although the current stress for those two phases is varied under different particle parameters, those varied current stresses are all within the SOA, which will not affect the stable operation and power quality performance of the WBG/Si HHB-based converters, and it is the premise and necessary condition for online adaptive PSO optimization.

### C. Adaptive Optimization Strategy

Fig. 5 shows the control strategy of the proposed adaptive power-sharing ratio and switching frequency control, which comprises the hybrid-frequency interleaving control (HFIC) and PSO optimization. The HFIC for HHB is used to coordinate those two phases' currents to achieve free power sharing and real-time ripple compensation. The detailed technical description of the HFIC can be found in our previous publication [1], and not repeated here.

The focus of the adaptive power-sharing ratio and switching frequency control is to select the optimal parameter with the PSO. In a real converter, the implementation steps for the proposed algorithm are listed as follows.

*Step 1:* Start the converter with the initial particle ($f_L$, $K_i$).
Step 2: Update and implement the particles with the PSO algorithm, and calculate the power loss with (9).
*Step 3:* Compare the power loss performance for different particles, and find the local best and global best particle.
*Step 4:* Generate new particles based on the comparison, and repeat steps 2-4 to find the optimal particle.
*Step 5:* When the optimal particle is founded, operate the converter with optimal parameters and record the optimal parameters into a LUT.

Fig. 6 shows the flowchart of the PSO optimal algorithm. At first, the initial parameters are loaded, which include the position and velocity limitation, and the limitation of position (limitation of the optimization variables) should be carefully selected to ensure the optimization ranges are all within the safe operation of the selected device. After loading the limitation parameters and learning factors, the initial particle position and velocity are set. Then, the particles are updated and implemented, as shown in the red box in Fig. 6.

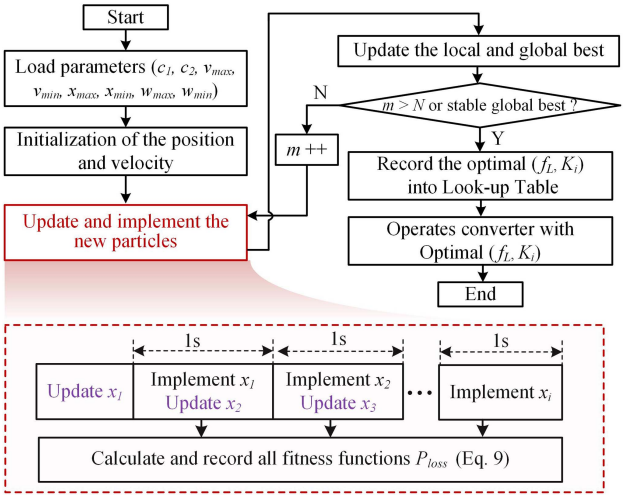


Fig. 6. Flowchart of the PSO optimal algorithm.

In the ac–dc inverter case study, the optimization period for power loss is in terms of the grid line cycle (50 Hz), which is aimed at minimizing the average power loss in one grid line cycle, and the calculation unit time for the power loss (fitness function) is long to 0.02 s. Meanwhile, the power loss under one single particle needs time to be characterized stably. When the implementation particle varies, the power loss and junction temperature of the devices are coupled to each other and only stabilize until they reach a thermal steady state, which requires a long implementation time for individual particles. Therefore, the implementation time in the proposed ac case study is chosen to be 1 s (50 gird line cycles) to temporarily obtain stable and accurate power loss data. While for dc applications, the port current and voltage are almost constant under one certain condition, the optimization unit and implementation cycle can be shortened.

Although the optimization time is 1 s, the switching frequency level variation can be measured in real time and well reflected in the calculation process of power loss, and the PSO optimization process will not affect the stable output current quality.

When the maximum number of iterations is reached or the global power loss best is stable, the optimal parameters are obtained, the optimization process is completed, and the converter will operate with the found optimal parameters. Then, a LUT can be built for the optimal parameters for different operating conditions. If the operation is later run to the same operating condition, the optimal data can be directly selected and run without repeated optimization, which can alleviate the problem of long optimization times for a single operation.

### D. Calculation Burden Analysis

To reduce the calculation requirements for the proposed PSO algorithm, a step-by-step calculation strategy is presented, which calculates the particles sequentially, rather than all at once in a control cycle.

Fig. 7 shows the implementation sequence for the step-by-step calculation strategy, in which the calculation burden of

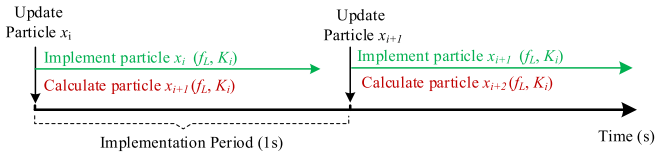


Fig. 7. Implementation sequence of the step-by-step calculation strategy.

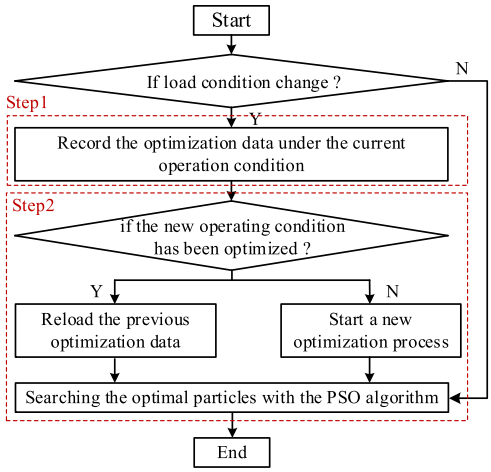


Fig. 8. Flowchart of incremental optimization for load-variation conditions.

calculating particle $x_{i+1}$ is averaged to the cycle (1 s) of operating particle $x_i$. The calculation task of particle $x_{i+1}$ only needs to be completed within this period (1 s), so the average number of calculations per control cycle is very small, which greatly reduces the real-time calculation requirements for the controller.

For example, according to the expression of updating particle, the calculation burdens of updating the position and velocity of a single-dimensional particle only require 12 basic calculations. Considering 2–5 dimensions in a single particle, the total calculation times for updating a single particle is 24–60. These calculations only need to be completed within the last implementation stage (1 s), so the calculation task of obtaining a new particle can be completed by only adding at most one basic calculation in each single control cycle, which will not affect the normal operation of the controller.

### E. Discussion for Load-Variation Conditions

When the load changes, an incremental optimization method is adopted for the PSO algorithm, and its flowchart is shown in Fig. 8, which can be divided into two steps.

*Step 1:* The PSO records the optimization data under the current operating conditions, including the PSO internal parameters, particle data, and operating conditions, to obtain the last optimal data for the next operation under the same operating conditions or to continue the optimization, which can avoid repeated optimization for the same operating conditions.

*Step 2:* The PSO queries whether there is already an optimization record for this new condition before, and if so, loads the previous data (internal parameters and particle data) to continue the

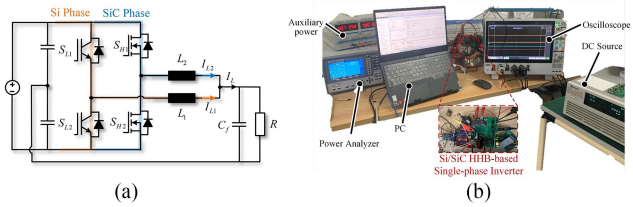


Fig. 9. HHB-based single-phase inverter. (a) Topology. (b) Laboratory platform.

TABLE I
HARDWARE PARAMETERS OF SI/SIC HHB-BASED INVERTER

| Parameters | Value |
|---|---|
| Input Voltage | DC 400 V |
| Rated Power | 3kW |
| Si Phase | Si IGBT IKW40N65H5 |
| SiC Phase | SiC MOS IMW65R107 |
| Inductor $L_1$ | 1mH |
| Inductor $L_2$ | 250uH |
| Output filter Capacitor $C_f$ | 2uF |
| SiC Phase Switching Frequency | Fixed 100kHz |

previous optimization. If not, restarts an optimization process to find the optimal parameters for this new condition.

Through the proposed incremental optimization, when the load keeps changing so fast that the PSO does not have enough time to obtain the optimal parameters, the optimal parameters can be obtained in steps by multiple incremental optimizations. Meanwhile, the optimization process for the same operating condition can be performed only once by establishing the optimal parameters LUT under different operations, without repeated optimization.

## IV. EXPERIMENT RESULTS

In this section, a Si/SiC HHB-based single-phase inverter is selected as a case study, to validate the proposed optimization strategy. The topology diagram is plotted in Fig. 9(a), the detailed hardware parameters are summarized in Table I, and the details design guidelines for WBG/Si HHB inductors can be founded in [1] and [9]. The Si phase is made by the two Si IGBTs with an antiparallel diode (Infineon IKW40N65H5), and the SiC phase is made by two SiC MOSFETs (Infineon IKW65R107). The photo of the experimental platform is shown in Fig. 9(b), which consists of the dc source, power analyzer (Zimmer LMG540), FPGA controller (Xilinx AX7102), the test prototype, load cabinet, and oscilloscope. The current sampling circuit uses a TI AMC1301 isolation amplifier, whereas the voltage sampling circuit uses a TI TL082 amplifier. The ADC chip uses the conventional AD7606 with a 200 kHz sampling rate. Therefore, the sampling feedback for the full path can meet the requirement of accurate acquisition of Si-phase current ripple (10–30 kHz) to implement the proposed control strategy.

The controller uses a double closed control loop (voltage outer loop and current inner loop) to ensure that the output ac voltage rms value is maintained at 120 V, and the actual modulation index is around 0.84. The proposed control will adaptively select the

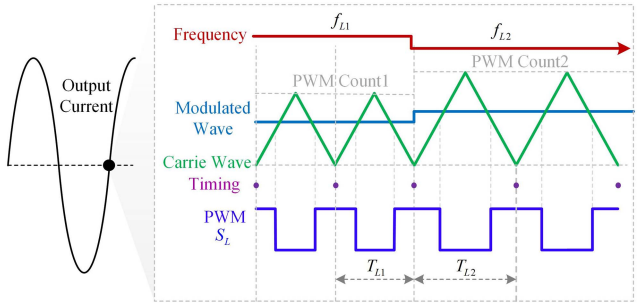


Fig. 10. Detailed implementation of the variable-frequency process.

combination of Si phase frequency $f_L$ and the power-sharing ratio $K$ to minimize the power loss under the current operating conditions. In addition, due to the wide range of optimization range for $f_L$, the following points should be carefully considered to ensure safe operation and implementation.

1) Each particle is updated near the ac zero-crossing point, and the voltage and current are low at this time, which can minimize the influence on the normal operation of the converter. Meanwhile, the synchronous modulation method is adopted, i.e., the sampling and calculation frequency is matched to its switching frequency. Therefore, the WBG phase sampling and control frequency is fixed in line with its' switching frequency, i.e., 100 kHz. While the Si phase sampling and control frequency is varied as its' switching frequency (10-30 kHz). The detailed implementation of the variable Si phase switching frequency process is shown in Fig. 10, and the frequency variation is implemented as the update of the PWM count. The frequency updating, sampling, and calculation timing of each cycle are carried out at the starting point of each triangular carrier wave to ensure stable operation, as shown by the purple point in Fig. 10.
2) When there are more than one power-sharing ratio parameters $K_i$, the $K$ is selected based on the absolute value of the reference current $I_{Lr}$. Taking the 3-D particle in Fig. 4 as an example, the segmental expression for the power-sharing ratio can be expressed as follows:

$$K = \begin{cases} K_1, \textbf{if } |I_{Lr}| < I_m/2 \\ K_2, \textbf{if } |I_{Lr}| > I_m/2 \end{cases} \tag{15}$$

where $I_{Lr}$ represents the input current reference value, and $I_m$ is the amplitude of the $I_{Lr}$.

3) The system stability under different Si phase switching frequencies $f_L$ should be analyzed. The Si phase operation can be seen as a conventional variable-frequency inverter, according to [24], and the discrete small-signal model for a single-phase inverter can be expressed as

$$F(z) = \frac{f_{\text{out}}(z)}{f_{\text{in}}(z)} = \frac{RT_L^2 z^2 + 2RT_L^2 z^2 + 1}{Az^2 + Bz + C} \tag{16}$$

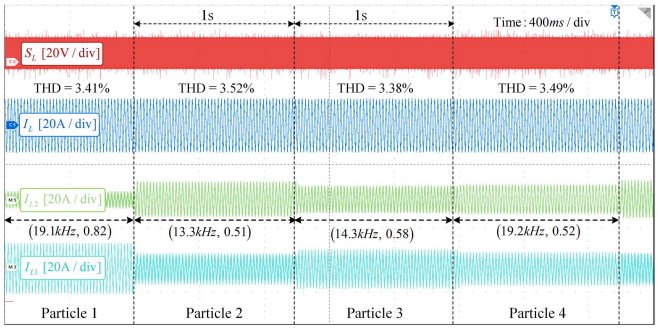


Fig. 11. Experimental waveforms during the optimization process of the 2-D PSO algorithm.

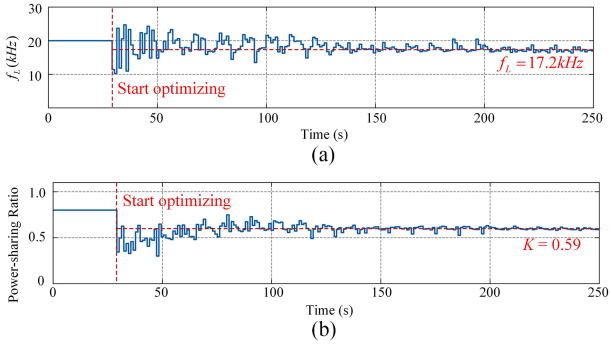


Fig. 12. Iterative process curve of particles in a 2-D PSO algorithm. (a) Si phase switching frequency. (b) Power-sharing ratio.

where $T_L$ stands for the Si phase switching cycle, and

$$\begin{cases} A = 4C_f L_1 R + 2L_1 T_L + RT_L^2 \\ B = 2RT_L^2 - 8C_f L_1 R \\ C = 4C_f L_1 R - 2L_1 T_L + RT_L^2 \end{cases} \tag{17}$$

where $C_f$, $L_1$, and $R$ stand for the output filter capacitor, Si phase inductance, and output load. To ensure the stability state under the whole optimization range, the modulus of the characteristic roots of $f_{in}(z)$ must all be small than 1 under different switching frequencies [23], and the characteristic roots of the $f_{in}(z)$ can be expressed as

$$\begin{cases} z_1 = \frac{-B+\sqrt{B^2-4AC}}{2A} \\ z_2 = \frac{-B-\sqrt{B^2-4AC}}{2A}. \end{cases} \tag{18}$$

Subtracting the system parameters into (18), the results indicate that there are always $|z_1|<1$ and $|z_2|<1$ when the switching frequency is varied from 10–30 kHz under the full load range, which indicates that the inverter system is always stable under the whole frequency optimization range.

Fig. 11 shows the experimental waveforms of the proposed adaptive optimization process based on a 2-D PSO, where the input voltage is 400 V, the load is 1.5 kW, $c_1 = 2$, $c_2 = 2$, and $w = [0.4, 0.9]$. The number of particles is ten. The implementation time for each particle is 1 s. It can be seen that the total current total harmonic distortion (THD) remains almost constant under different particles, which indicates that the optimization process does not affect the output quality of the HHB, and it is a prerequisite condition for online optimization. In addition, the iterative process data of the PSO particles are extracted using the upper computer software, as shown in Fig. 12. After setting the initial parameters (20 kHz, 0.8), the Si-phase switching frequency $f_L$ stabilizes to 17.2 kHz by an optimization-seeking iteration, whereas the power-sharing ratio $K$ stabilizes to 0.59. The power loss is reduced from an initial 29.65 to 24.3 W, which demonstrates the effective loss-reduction ability of the proposed adaptive power-sharing ratio and switching frequency control.

To obtain the minimum power loss, the optimal internal parameters ($c_1$, $c_2$, $w_{\max}$, and $w_{\min}$) in the PSO algorithm are selected first. The optimization objective of this article is power loss, which can be equated to a single-peak problem under one optimization interval, and the mechanism of influence of initial parameters on optimization results is relatively simple, which can be selected by comparing the optimization results under several sets of initial parameters. Table II summarizes the optimal losses obtained by different PSO parameters at a fixed output power of 2.2 kW, including the minimum, maximum, and average values of 10 times optimization experiments. First, the range of the weight coefficients is fixed to [0.4, 0.9], and several optimization experiments with different learning factors are carried out. The results show that the minimum average loss is obtained by adaptive optimization at the learning factors $c_1 = 1$ and $c_2 = 2$. Then, the learning factors are fixed to $c_1 = 1$ and $c_2 = 2$, and the weighting factors are changed. The results showed that the optimal range of weighting factors is [0.4,1.4]. Therefore, this set of PSO parameters ($c_1 = 1$, $c_2 = 2$, $w = [0.4, 1.4]$) is chosen for subsequent experimental studies. After selecting the optimal learning factor and weight parameters, experiments with different particle dimensions are carried out.

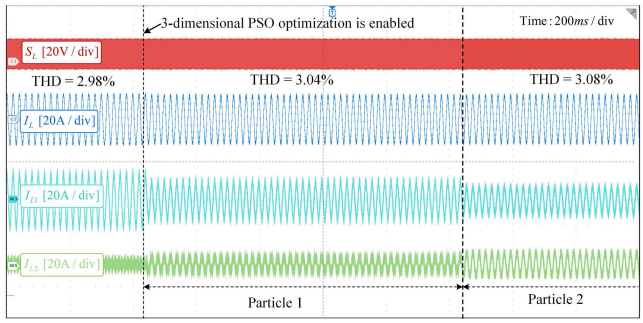


Fig. 13. Experimental waveforms during the optimization process of the 3-D PSO algorithm.

Fig. 13 shows the experimental waveform before and after investing in a 3-D particle optimization ($f_L$, $K_1$, and $K_2$). It can be seen that there is no abnormal current overshoot in all the currents under the transition process of the adoption of different 3-D particles, which indicates that the proposed adaptive optimization control does not affect the normal operation of the converter. Fig. 14 shows the details waveforms of a single 3-D particle implementation process. The adoption of multiple power-sharing ratio parameters in a line cycle may result in worse THD for the Si phase current, but the power quality of the total current is always ensured by the SiC phase high-frequency

TABLE II
LOSS COMPARISON OF HHB UNDER DIFFERENT PSO PARAMETERS, AND THE POWER LEVEL IS 2.2 KW

| Learning factors $c_1, c_2$ | weight factors $w$ | Maximum Loss | Minimum Loss | Average loss |
|---|---|---|---|---|
| $c_1 = 2, c_2 = 2$ | [0.4, 0.9] | 45.1W | 42.8W | 44.2W |
| $c_1 = 2, c_2 = 1$ | | 48.2W | 44.3W | 46.3W |
| $c_1 = 1, c_2 = 2$ | | 44.3W | 40.1W | 42.3W |
| $c_1 = 1, c_2 = 1$ | | 46.8W | 45.4W | 45.8W |
| $c_1 = 1, c_2 = 2$ | [0.4, 1.4] | 42.2W | 40.5W | 41.9W |
| | [0.4, 1.6] | 49.8W | 47.4W | 48.3W |
| | [0.2, 0.9] | 47.5W | 44.5W | 45.9W |
| | [0.2, 1.2] | 49.1W | 44.4W | 46.2W |

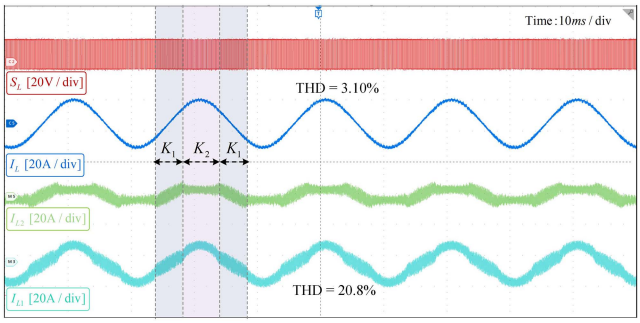


Fig. 14. Experimental waveforms of the implementation process of a single 3-D particle.

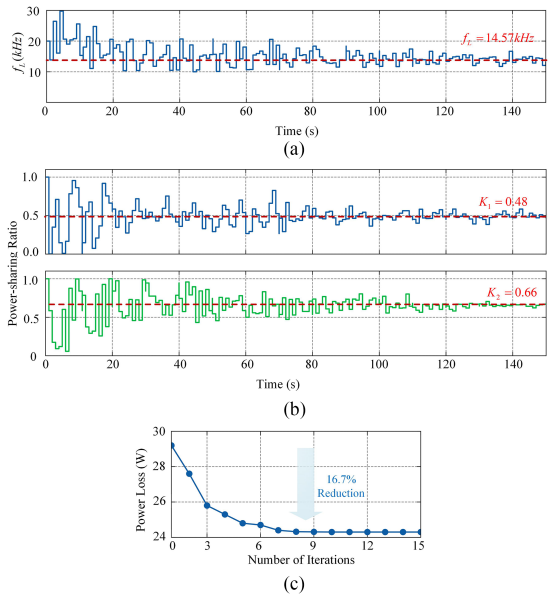


Fig. 15. Iterative process curve of particles in a 3-D PSO algorithm. (a) Si phase switching frequency. (b) Power-sharing ratio. (c) Global-best power loss.

operation, which exhibits comparable performance to the initial 2-D particle.

Fig. 15 shows the particle iteration process curve of the PSO algorithm for 3-D particles. After several iterations of the optimization search, the Si phase switching frequency is stabilized to 14.57 kHz, and the power-sharing ratio near the over-zero range is stabilized to 0.48, whereas the power-sharing ratio near the peak current region is larger, which is 0.66. Due to the low current in the over-zero range, the ON-state knee voltage of the Si IGBT and the equivalent resistance of the inductor $L_1$ has a large impact on the overall loss of the HHB, and thus, the $K$ chooses a smaller value to allow the SiC phase processes more current, obtaining a high efficiency. With the current increase, the influence of the ON-state knee voltage is reduced, and the $K$ near the peak current range is larger to allow the Si phase to process most of the total current to reduce switching losses. The corresponding global-best power loss is plotted in Fig. 15(c). When all the particles (ten particles needs 10 s) under one iteration have been implemented, the global-best power loss can be found by comparing the power loss under different particles. From Fig. 15(c), it can be found that the optimal loss stabilizes to 24.3 W after several iterations, achieving a 16.7% power loss reduction compared to the initial parameter of 29.2 W.

To validate the dynamic performance and effectiveness of the incremental optimization, the experiment under continuous load variation conditions is carried out. Fig. 16(a) shows the dynamic waveforms under the continuous load variation (500W–1 kW–500 W). When the load fluctuates, although the PSO has not yet found the optimal parameters, there is no overshoot abnormal current in each phase during the transient process, obtaining an excellent dynamic performance. The iterative process curve for incremental optimization is plotted in Fig. 16(b). Before the PSO finds the optimal parameters for the present operating condition (500 W), the load operating condition varies from 500 W to 1 kW. At this time, the PSO first stores the data of the optimization process in 500 W operating conditions and starts a new PSO optimization process for 1 kW load conditions. When the load current varies back to 500 W, the PSO reloads the previously stored data and continues the optimization process under the 500 W condition to find the optimal particle. The optimization process for the 500 W operating condition can be completed by the two-step optimization and finally convergence to the optimal parameters (21.3 kHz, 0.89), which verifies the effectiveness of the incremental optimization method.

Table III summarizes the power loss comparison under different particle dimensions, and the power level is 3 kW. When the particle dimension increases from 2 to 3, the overall loss of the converter decreases from 69.3 to 64.5 W. However, when the particle dimension continues to increase, the trend of loss reduction is not obvious. Considering the higher dimension will lead to an excessive computational burden on the controller, the subsequent experiments are carried out with 3-D particles.

TABLE III
LOSS COMPARISON OF HHB UNDER DIFFERENT PARTICLE DIMENSIONS, AND THE POWER LEVEL IS 3 KW

| Particle Dimension | Optimal Particle | Maximum Loss | Minimum r Loss | Average loss |
|---|---|---|---|---|
| Fixed Parameters (20kHz, 0.8) | / | 75.6W | 75.6W | 75.6W |
| 2-d ($f_L$, $K_1$) | (15.52kHz, 0.62) | 72.8W | 68.4W | 69.3W |
| 3-d ($f_L$, $K_1$, $K_2$) | (14.57kHz, 0.48, 0.66) | 66.2W | 63.1W | 64.5W |
| 4-d ($f_L$, $K_1$, $K_2$, $K_3$) | (14.55kHz, 0.44, 0.53, 0.67) | 65.4W | 63.5W | 64.0W |
| 5-d ($f_L$, $K_1$, $K_2$, $K_3$, $K_4$) | (14.6kHz, 0.32, 0.45, 0.61, 0.74) | 66.3W | 63.2W | 64.1W |

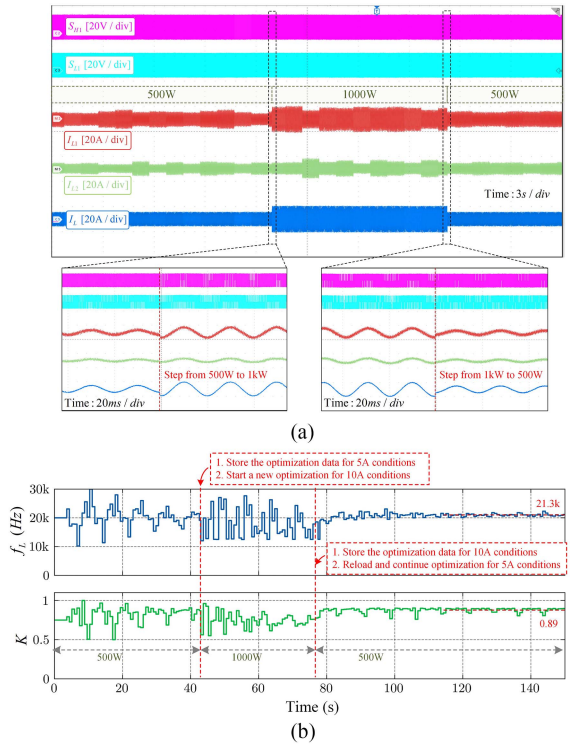


Fig. 16. Dynamic experimental for load variation conditions. (a) Dynamic experimental waveforms. (b) Iterative process curves for incremental optimization.

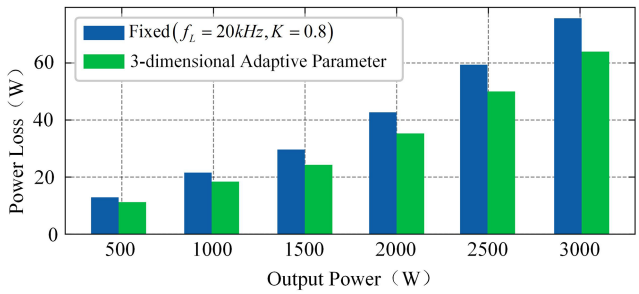


Fig. 17. Power loss comparison between the fixed parameters and 3-D PSO adaptive parameters.

Fig. 17 shows the power loss comparison between 3-D particles and fixed parameters at different output powers. It can be seen that the proposed adaptive control can reduce the power loss across the entire load range and achieve a maximum loss reduction of 18% at 1.5 kW, which verifies the effectiveness of the proposed adaptive control.

## V. CONCLUSION

In this article, a novel adaptive power-sharing ratio and switching frequency control adopting the PSO algorithm is proposed for WBG/Si HHB. The proposed method can easily and effectively search the optimal parameters under different operation conditions without additional intervention and hardware, obtaining strong adaptability. The proposed method does not require real-time complex calculations, it only needs to be calculated the fitness function. Meanwhile, by properly selecting the optimal parameters, the power quality will not be affected during the optimization process. Further, the computation burden and incremental optimization for variable-load conditions are presented. An experimental platform of the HHB-based 3 kW Si IGBT /SiC MOS single-phase inverter is set up and tested to highlight the benefits of the proposed adaptive parameters control. Compared with the fixed parameters, the proposed adaptive approach can achieve a power loss reduction across the entire load range conditions without any extra components, a maximum losses reduction of up to 18%, which is of great significance for fully exploiting the advantages of the WBG/Si HHB converter.

## REFERENCES

[1] C. Zhang et al., "WBG and Si hybrid half-bridge power processing toward optimal efficiency, power quality, and cost tradeoff," *IEEE Trans. Power Electron.*, vol. 37, no. 6, pp. 6844–6856, Jun. 2022.
[2] T.-F. Wu, Y.-H. Huang, S. Temir, and C.-C. Chan, "3Φ4W hybrid frequency parallel uninterruptable power supply for reducing voltage distortion and improving dynamic response," *IEEE J. Emerg. Sel. Top. Power Electron.*, vol. 10, no. 1, pp. 906–918, Feb. 2022.
[3] T.-F. Wu, Y.-H. Huang, and Y.-T. Liu, "3Φ4W grid-connected hybrid-frequency parallel inverter system with ripple compensation to achieve fast response and low current distortion," *IEEE Trans. Ind. Electron.*, vol. 68, no. 11, pp. 10890–10901, Nov. 2021.
[4] C. Liu et al., "Hybrid SiC-Si DC–AC topology: SHEPWM Si-IGBT master unit handling high power integrated with partial-power SiC-MOSFET slave unit improving performance," *IEEE Trans. Power Electron.*, vol. 37, no. 3, pp. 3085–3098, Mar. 2022.
[5] C. Zhang, X. Xie, K. Qu, B. Hu, Z. Li, and J. Wang, "A hybrid Si/SiC CCM interleaved totem-pole bridgeless PFC converter with coupled-inductor and hybrid-frequency interleaving operation," in *Proc. IEEE 1st Int. Power Electron. Appl. Symp.*, 2021, pp. 1–5.
[6] K. Qu, C. Zhang, W. Chen, B. Hu, J. Chen, and J. Wang, "A hybrid Si/SiC interleaved bidirectional DC-DC converter to optimal power quality, efficiency, and cost tradeoff," in *Proc. IEEE Energy Convers. Congr. Expo .*, 2021, pp. 2001–2004.
[7] T.-F. Wu, T. Sakavov, and Y.-H. Huang, "Current ripple compensation algorithm for paralleled three-phase three-wire hybrid frequency inverter systems," in *Proc. IEEE 12th Int. Symp. Power Electron. Distrib. Gener. Syst.*, 2021, pp. 1–5.
[8] C. Zhang et al., "A new PFC design with interleaved mhz-frequency GaN auxiliary active filter phase and low-frequency base power Si phase," *IEEE J. Emerg. Sel. Top. Power Electron.*, vol. 8, no. 1, pp. 557–566, Mar. 2020.

[9] C. Zhang et al., "WBG partial power processing: A new PFC design with interleaved mhz-frequency GaN and low-frequency Si phases," in *Proc. IEEE Energy Convers. Congr. Expo.*, 2019, pp. 2702–2706.
[10] A. Kundu, R. Na, A. Amir, Y. Zhou, I. P. Brown, and Z. J. Shen, "WBG fractional power processing: A new Si-SiC hybrid voltage source inverter design," in *Proc. IEEE Energy Convers. Congr. Expo.*, 2020, pp. 6226–6231.
[11] A. Kundu, R. Na, A. Amir, and Z. J. Shen, "Optimization strategy of WBG fractional power processing," in *Proc. IEEE Appl. Power Electron. Conf. Expo.*, 2021, pp. 896–901.
[12] C. Zhang, K. Qu, B. Hu, J. Wang, X. Yin, and Z. J. Shen, "A high-frequency dynamically coordinated hybrid Si/SiC interleaved CCM totem-pole bridgeless PFC converter," *IEEE J. Emerg. Sel. Top. Power Electron.*, vol. 10, no. 2, pp. 2088–2100, Apr. 2022.
[13] W. Chen, C. Zhang, K. Qu, B. Hu, J. Chen, and J. Wang, "A new hybrid Si/SiC CCM totem pole bridgeless PFC design towards optimal performance and cost tradeoff," in *Proc. IEEE Energy Convers. Congr. Expo.*, 2021, pp. 2203–2207.
[14] C. Zhang, X. Yuan, J. Wang, B. Hu, X. Yin, and Z. J. Shen, "Optimization of power sharing and switching frequency in Si/WBG hybrid half-bridge converters using power loss models," *IEEE J. Emerg. Sel. Top. Power Electron.*, early access, Dec. 6, 2022, doi: 10.1109/JESTPE.2022.3226196.
[15] Z. Peng et al., "Adaptive gate delay-time control of Si/SiC hybrid switch for efficiency improvement in inverters," *IEEE Trans. Power Electron.*, vol. 36, no. 3, pp. 3437–3449, Mar. 2021.
[16] M. Schubert and R. W. D. Doncker, "Semiconductor temperature and condition monitoring using gate-driver-integrated inverter output voltage measurement," *IEEE Trans. Ind. Appl.*, vol. 56, no. 3, pp. 2894–2902, May/Jun. 2020.
[17] MAGNETICS, 2022. [Online]. Available: https://www.mag-inc.com
[18] R. Eberhart and J. Kennedy, "A new optimizer using particle swarm theory," in *Proc. IEEE 6th Int. Symp. Micro Mach. Hum. Sci.*, 1995, pp. 39–43.
[19] G. L. Torres and V. H. Quintana, "On a nonlinear multiple-centrality-corrections interior-point method for optimal power flow," *IEEE Trans. Power Syst.*, vol. 16, no. 2, pp. 222–228, May 2001.
[20] Y. Wang et al., "Minimum-current-stress scheme of three-level dual active bridge DC-DC converters with the particle swarm optimization," *IEEE Trans. Transp. Electrific.*, vol. 7, no. 4, pp. 2067–2084, Dec. 2021.
[21] M. Jafari, Z. Malekjamshidi, and M. R. Islam, "Optimal design of a multiwinding high-frequency transformer using reluctance network modeling and particle swarm optimization techniques for the application of PV-linked grid-connected modular multilevel inverters," *IEEE J. Emerg. Sel. Top. Power Electron.*, vol. 9, no. 4, pp. 5083–5096, Aug. 2021.
[22] K. Hamdaoui and A. Charef, "A new discretization method for fractional order differentiators via the bilinear transformation," in *Proc. IEEE 15th Int. Conf. Digit. Signal Process.*, Jul. 2007, pp. 280–283.
[23] J.-H. Lee and J.-S. Du, "Phase characteristics for the stability of 2-D quarter-plane recursive digital all-pass filters," *IEEE Trans. Circuits Syst. II, Exp. Briefs*, vol. 63, no. 3, pp. 289–293, Mar. 2016.
[24] Z. Peng, J. Wang, Z. Liu, Y. Dai, G. Zeng, and Z. J. Shen, "Fault-tolerant inverter operation based on Si/SiC hybrid switches," *IEEE J. Emerg. Sel. Top. Power Electron.*, vol. 8, no. 1, pp. 545–556, Mar. 2020.

**Chao Zhang** (Member, IEEE) received the B.S. degree in electrical engineering and automation from Guizhou University, Guiyang, China, in 2017, and the Ph.D. degree in electrical engineering from Hunan University, Changsha, China, in 2022.

He is currently a Lecturer with Electrical Engineering College, Guizhou University. His research focuses on wide bandgap semiconductors and applications.

**Xufeng Yuan** (Member, IEEE) received the Ph.D. degree in electrical engineering from the Huazhong University of Science and Technology (HUST), Wuhan, China, in 2007.

He is currently a Professor with Electrical Engineering College, Guizhou University, Guiyang, China. His research interests include renewable energy generation systems and power system control.

**Jun Wang** (Senior Member, IEEE) received the B.S. degree from the Huazhong University of Science and Technology, Wuhan, China, in 2000, the M.S. degree from the Institute of Semiconductors, Chinese Academy of Sciences, Beijing, China, in 2003, the M.E. degree from the University of South Carolina, Columbia, SC, USA, in 2005, and the Ph.D. degree from North Carolina State University, Raleigh, NC, USA, in 2010, all in electrical engineering.

Between 2010 and 2013, he was a device design engineer with Texas Instruments, Inc., Bethlehem, PA, USA. In 2014, he became a Professor with the College of Electrical and Information Engineering, Hunan University, Changsha, China, in 2014. His research interests include power semiconductor devices and their applications in power electronics systems.

Dr. Wang has been an Associate Editor of the IEEE JOURNAL OF EMERGING AND SELECTED TOPICS IN POWER ELECTRONICS since 2017.

**Weibin Chen** received the B.S. degree in electrical engineering in 2020 from the College of Electrical and Information Engineering, Hunan University, Hengyang, China, where he is currently working toward the M.S. degree in electrical engineering.

His research focuses on power semiconductor devices and their applications.

**Bo Hu** (Graduate Student Member, IEEE) received the B.S. and M.S. degrees in automation from the College of Electrical Engineering, University of South China, Hengyang, China, in 2014 and 2017, respectively. He is currently working toward the Ph.D. degree in electrical engineering with Hunan University, Changsha, China.

His research focuses on power semiconductor devices and their applications.

**Zheng John Shen** (Fellow, IEEE) received the B.S. degree from Tsinghua University, Beijing, China, in 1987, and the M.S. and Ph.D. degrees from Rensselaer Polytechnic Institute, Troy, NY, USA, in 1991 and 1994, respectively, all in electrical engineering.

Between 1994 and 1999, he held a variety of positions, including Senior Principal Staff Scientist with Motorola, Chicago, IL, USA. He was on Faculty of the University of Michigan-Dearborn, Dearborn, MI, USA, between 1999 and 2004, and the University of Central Florida, Orlando, FL, USA, between 2004 and 2012. He joined the Illinois Institute of Technology, Chicago, IL, USA, in 2013 as the Grainger Chair Professor in Electrical and Power Engineering. He has also held a courtesy professorship with Hunan University, Changsha, China, since 2007, and with Zhejiang University, Hangzhou, China, since 2013. His research interests include power electronics, power semiconductor devices and ICs, automotive electronics, renewable and alternative energy systems, and electronics manufacturing.

Dr. Shen was the recipient of the 2012 IEEE Region 3 Outstanding Engineer Award, 2003 NSF CAREER Award, 2006 IEEE Transaction Paper Award from IEEE Society of Power Electronics, 2003 IEEE Best Automotive Electronics Paper Award from the IEEE Society of Vehicular Technology, and 1996 Motorola Science and Technology Award. He was the VP of Products from 2009 to 2012, Associate Editor and Guest Editor-in-Chief of the IEEE TRANSACTIONS ON POWER ELECTRONICS, Technical Program Chair and General Chair of several major IEEE conferences.